Support information for

Ni nanoparticles @ Ni-Mo nitride nanorod arrays: a novel 3D-network hierarchical structure for high areal capacitance hybrid supercapacitors

Yunjun Ruan, Lin Lv, Zhishan Li, Chundong Wang, Jianjun Jiang**

School of Optical and Electronic Information, Huazhong University of Science and Technology, Wuhan 430074, P.R.China.

*Corresponding author E-mail: apcdwang@hust.edu.cn; jiangjj@mail.hust.edu.cn

Content

S1. Morphology and structure characterization.

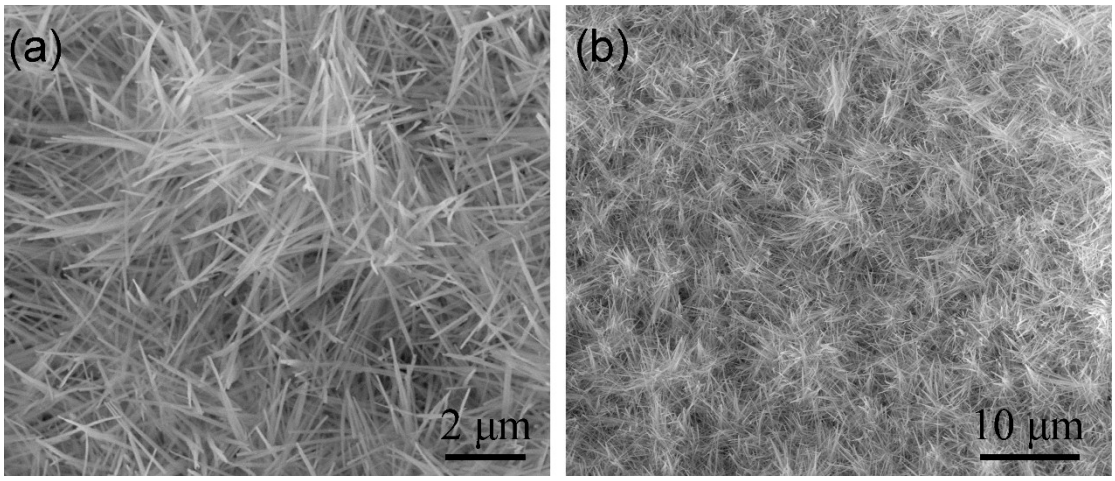

Fig. S1. SEM images of as-obtained $NiMoO_4$ precursor nanorods.

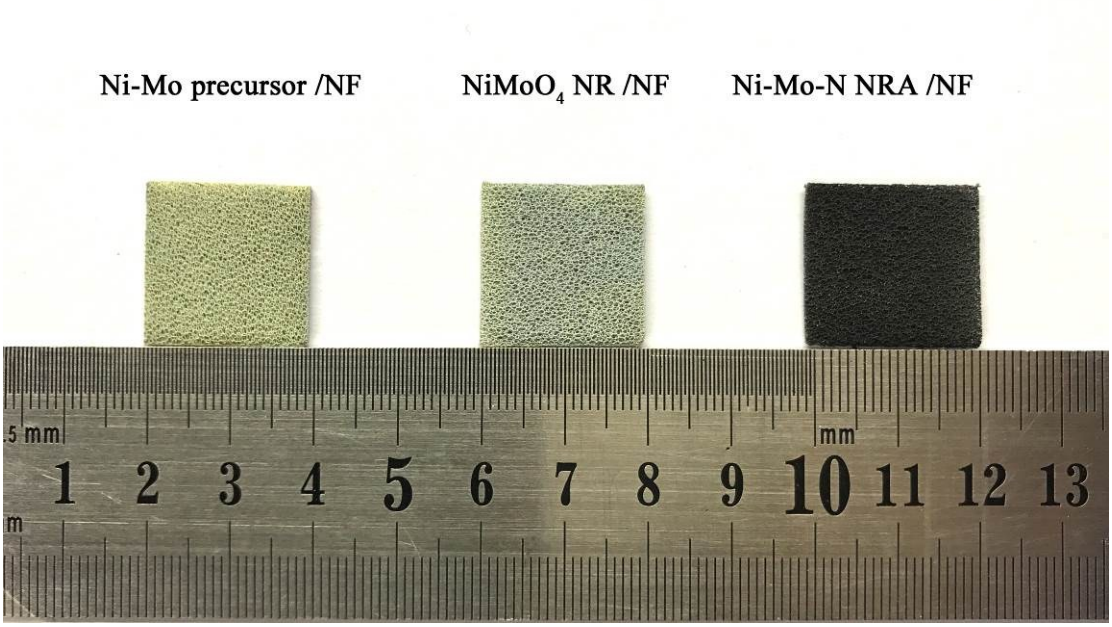

Fig. S2. The digital photograph of $NiMoO_4$ precursor/NF, $NiMoO_4$ NR/NF, and Ni-Mo-N NRA/NF.

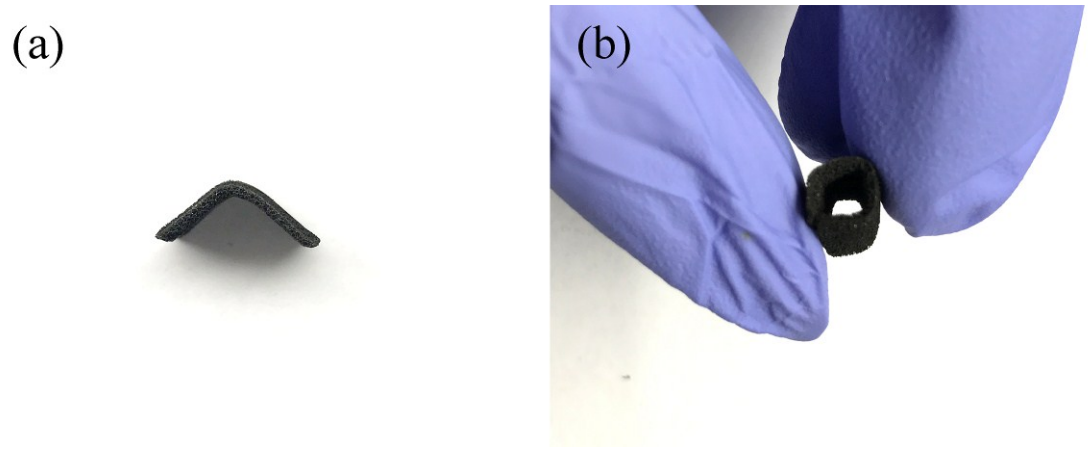

Fig. S3. The mechanical stability test of Ni-Mo-N NRA/NF: (a) bending to ca. 100 degree and (b) rolling into a tube.

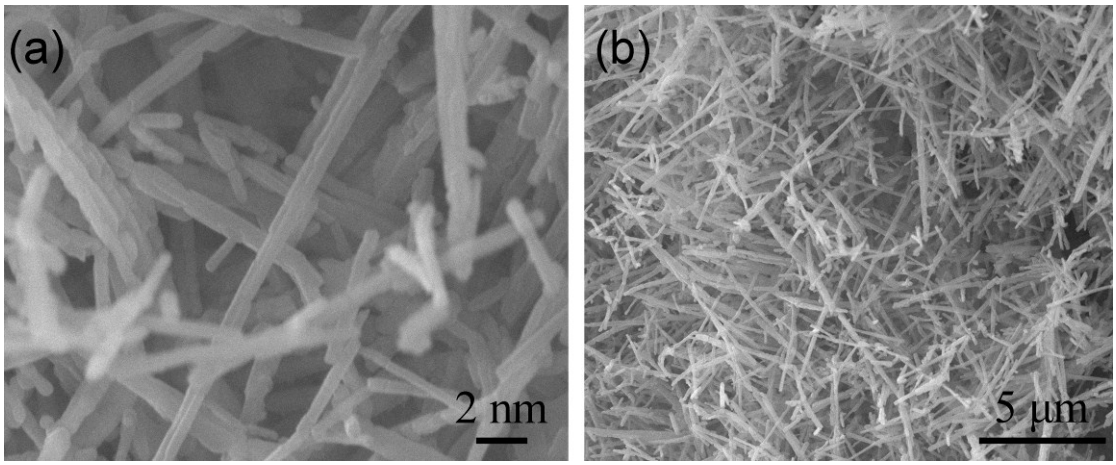

Fig. S4. SEM images of the as-obtained $NiMoO_4$ nanorods (annealing in air).

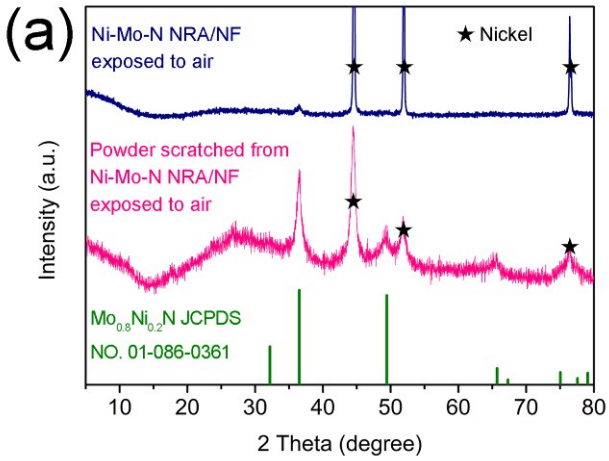

Fig. S5. XRD patterns of (a) Ni-Mo-N NRA/NF and the powders (scratched from NF) that was exposed to air at room temperature for 10 days.

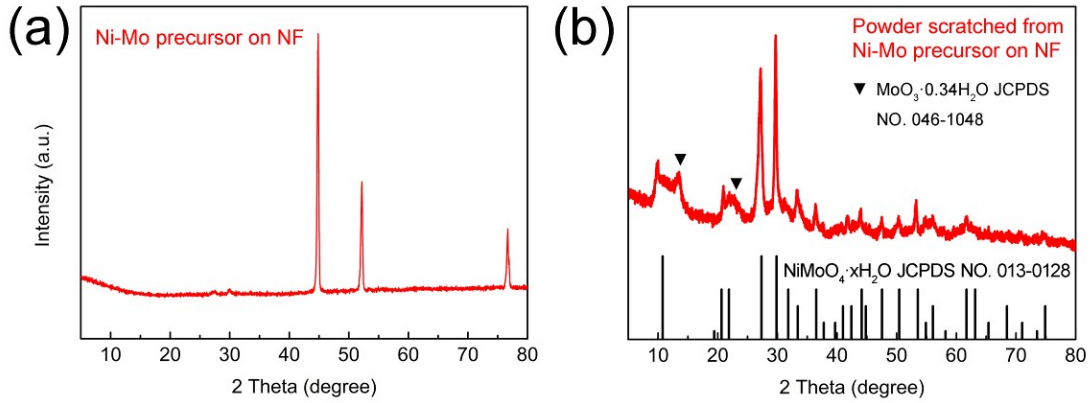

Fig. S6. XRD patterns of (a) Ni-Mo precursor on NF and (b) powder scratched from NF.

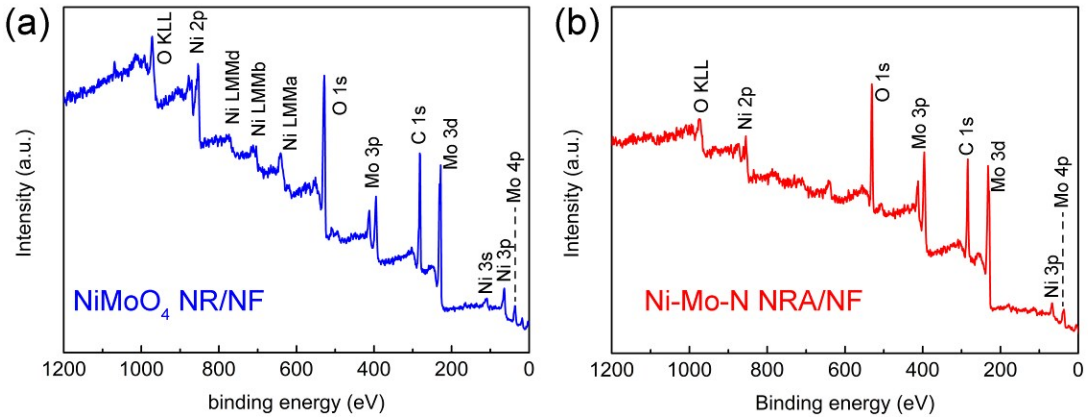

Fig. S7. XPS survey spectrums of (a) $NiMoO_4$ NR/NF and (b) Ni-Mo-N NRA/NF.

S2. Electrochemical performance of $NiMoO_4$ NR/NF and Ni-Mo-N NRA/NF electrodes.

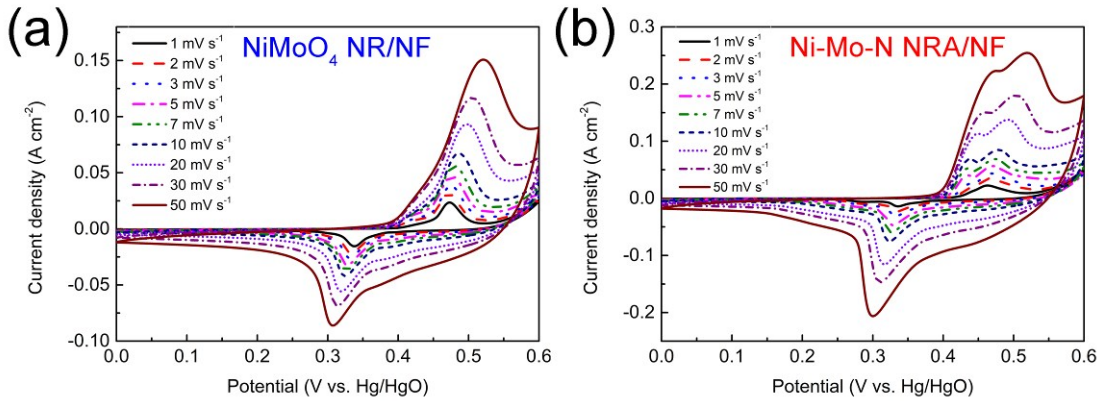

Fig. S8. CV curves at different scan rates. (a) $NiMoO_4$ NR/NF electrode. (b) Ni-Mo-N NRA/NF electrode.

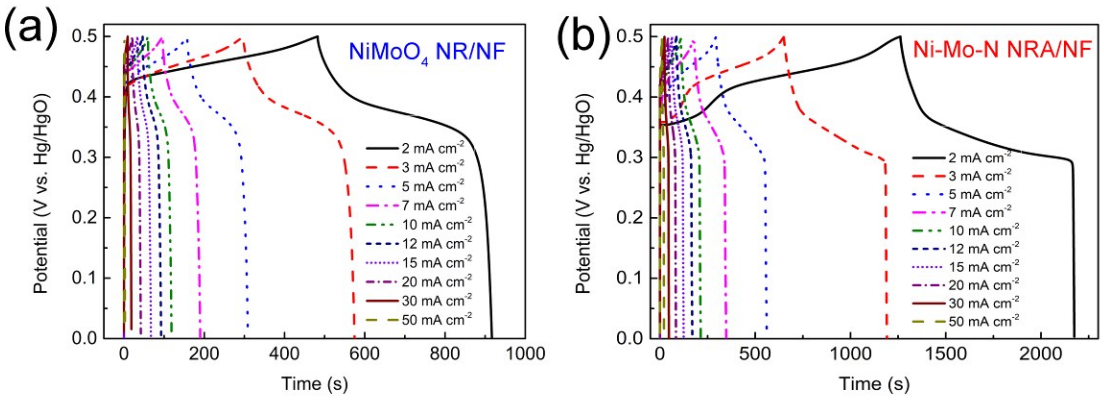

Fig. S9. GCD curves at different current densities. (a) $NiMoO_4$ NR/NF electrode. (b) Ni-Mo-N NRA/NF electrode.

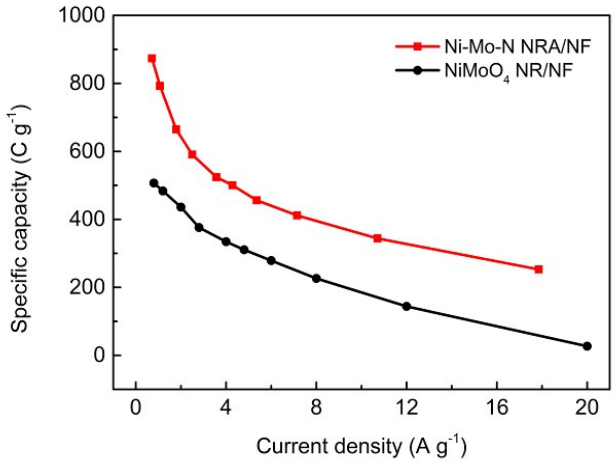

Fig. S10. Specific capacity of Ni-Mo-N NRA/NF and NiMoO4 NR/NF as a function of current density.

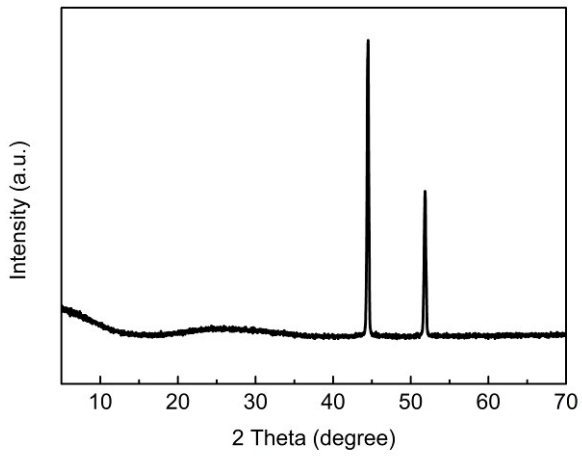

Fig. S11. XRD pattern Ni-Mo-N NRA/NF electrode after cycling test.

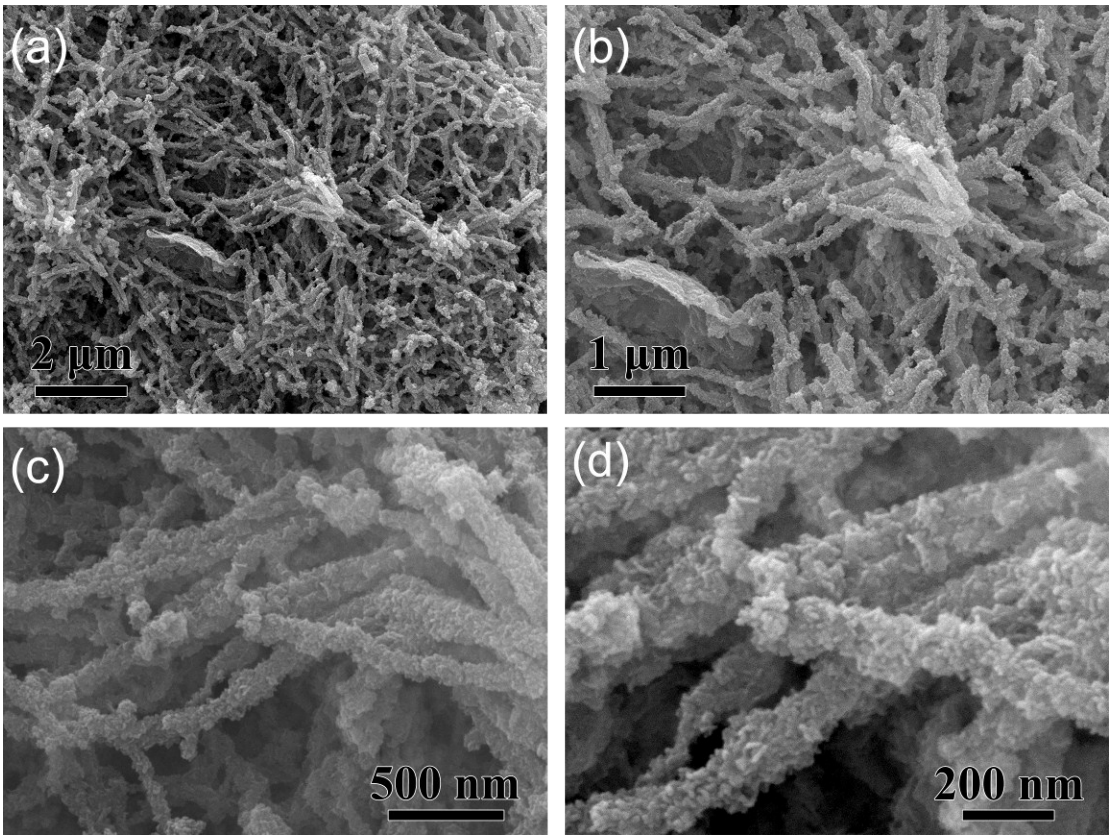

Fig. S12. SEM images of Ni-Mo-N NRA/NF after cycling test.

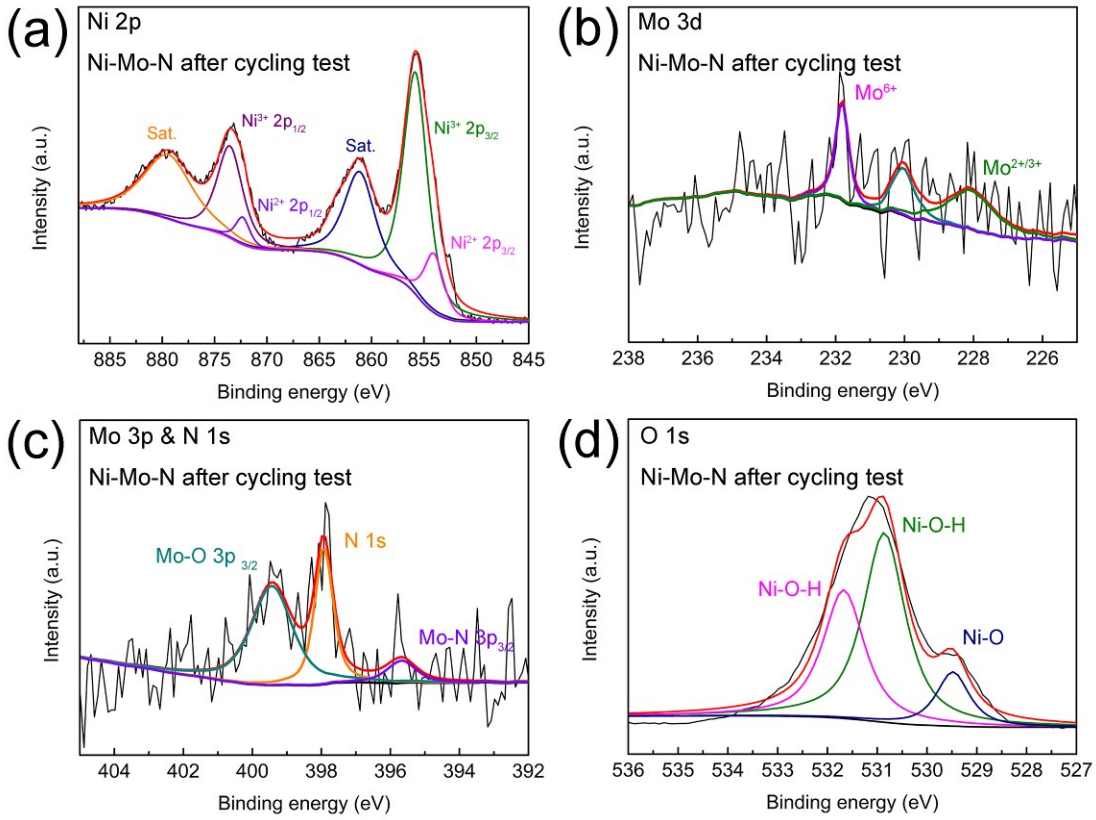

Fig. S13. XPS spectra of Ni-Mo-N NRA/NF after cycling test: (a) Ni 2p spectrum, (b) Mo 3d

spectrum, (c) Mo 3p and N 1s spectrum, and (d) O 1s spectrum.

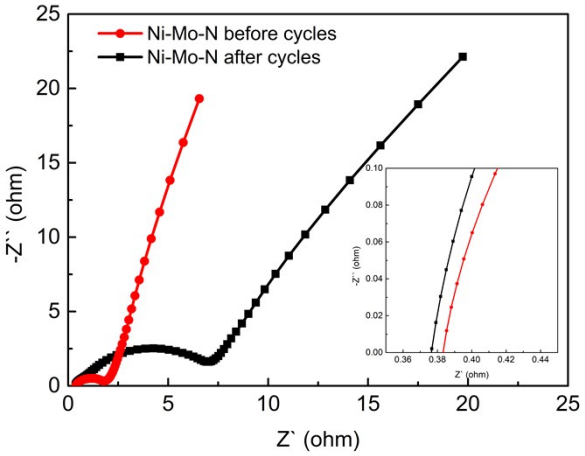

Fig. S14. Nyquist plots for Ni-Mo-N NRA/NF electrode before and after cycling test. The inset is the related enlarged Nyquist plots in the high frequency region.

S3. Electrochemical performance of supercapacitors.

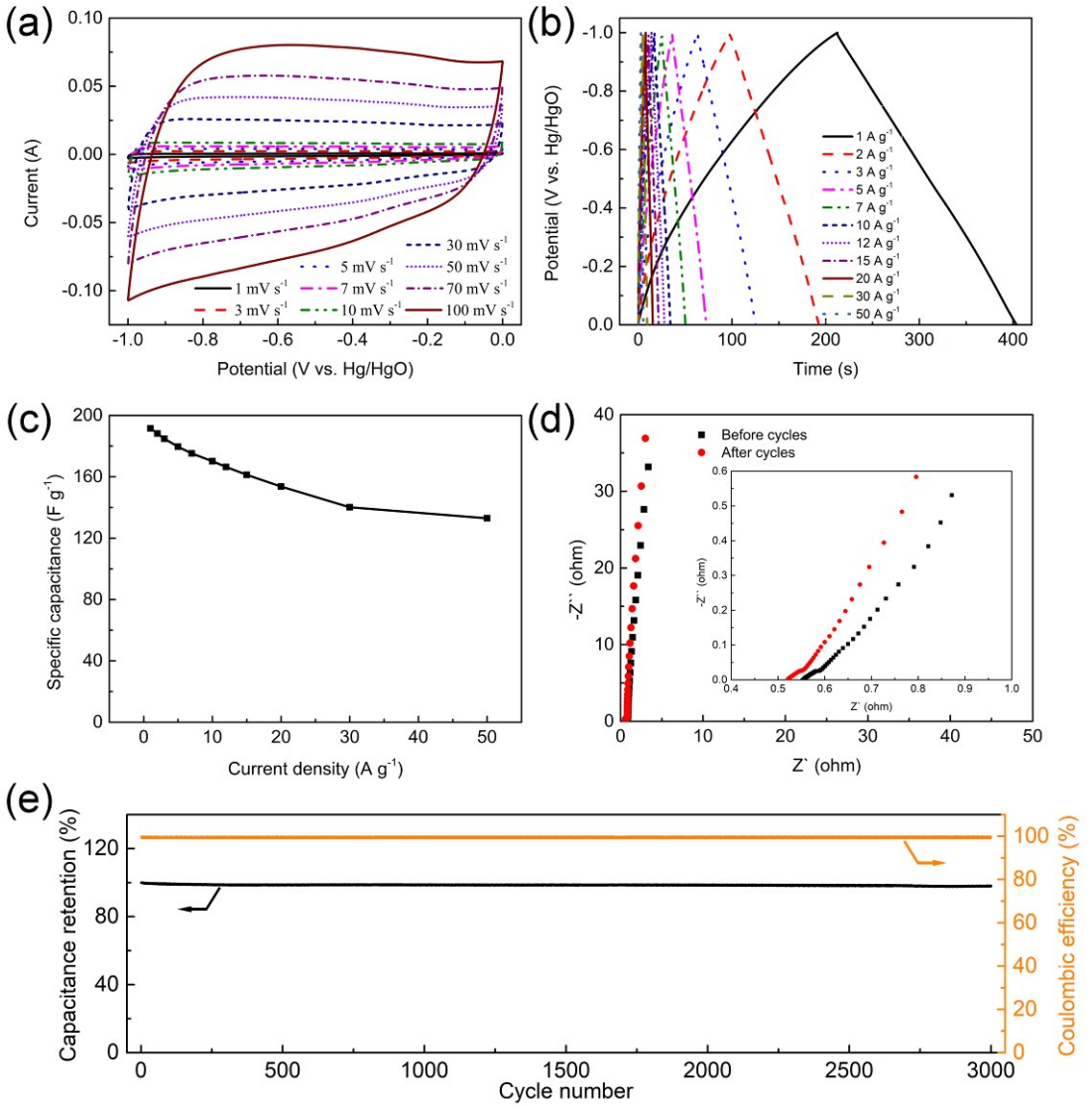

Fig. S15. Electrochemical performance of individual RGO electrode. (a) CV curves, (b) galvanostatic charge-discharge curves, (c) specific capacitance versus current density, (d) Nyquist plots (the inset is the enlarged high frequency region of Nyquist plots), and (e) cycling stability.

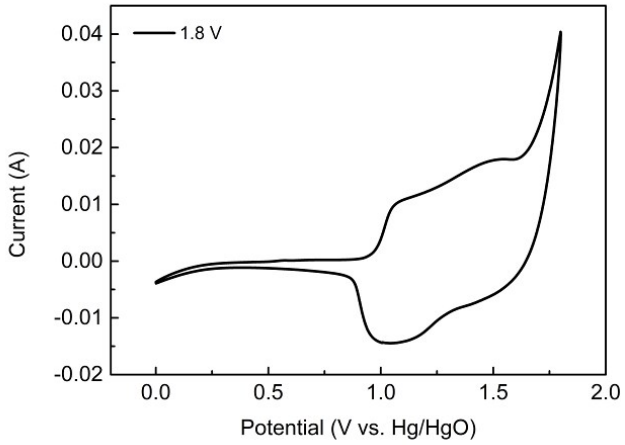

Fig. S16. CV curve of Ni-Mo-N NRA/NF in voltage window of 1.8 V at a scan rate of 10 mV s^{-1}.

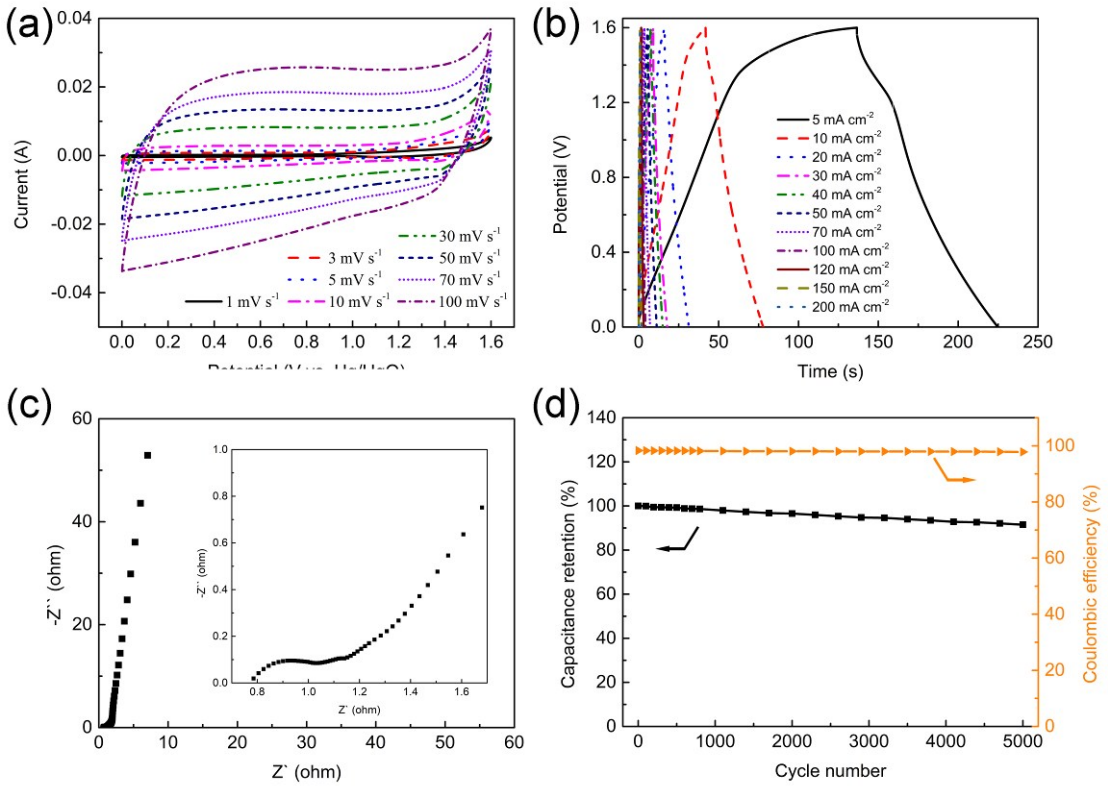

Fig. S17. Electrochemical performance of RGO//RGO symmetric supercapacitor. (a) CV curves, (b) galvanostatic charge-discharge curves, (c) Nyquist plots (the inset is the enlarged high frequency region of Nyquist plots), and (d) cycling stability.

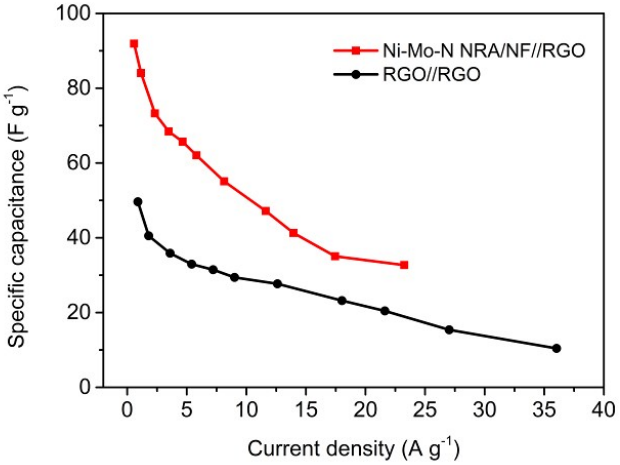

Fig. S18. Specific capacitance of Ni-Mo-N NRA/NF//RGO and RGO//RGO as a function of current density.

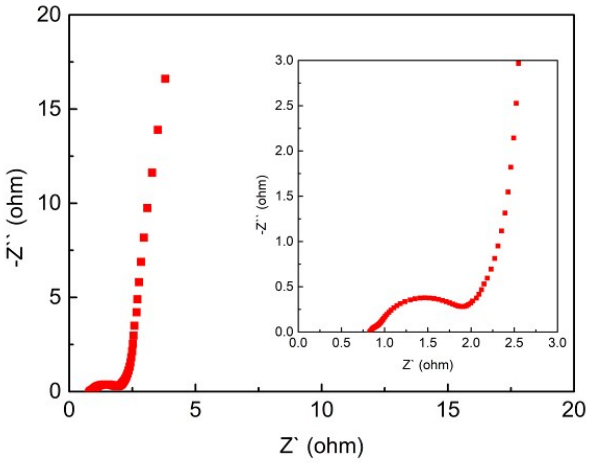

Fig. S19. Nyquist plots of Ni-Mo-N NRA/NF//RGO supercapacitor. The inset is the enlarged high frequency region of Nyquist plots.

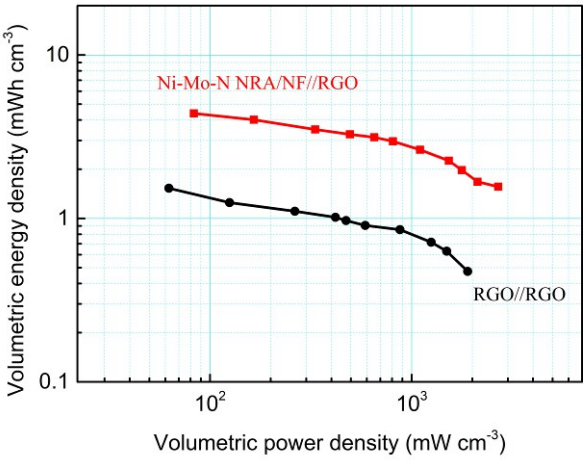

Fig. S20. Ragone plots of the supercapacitors.